Nano Research

Open Access

Research Article

Electrostatic attraction-directed membrane anchoring as a universal tool to enhance nanocarrier uptake into drug-resistant cancer cells

Qixiao Guan[1], Rong Chen[2,3], Zhengtao Tian[1], Peipei Zhang[1], Lingshan Liu[1], Meng Cheng[1], Yirong Zeng[1], Daikun Wu[1], Min Zhou[2,3] ✉, and Hongjing Dou[1] ✉

[1] *The state Key Laboratory of Metal Matrix Composites, School of Materials Science and Engineering, Shanghai Jiao Tong University, Shanghai 200240, China*
[2] *Department of Respiratory and Critical Care Medicine, Ruijin Hospital, Shanghai Jiao Tong University School of Medicine, Shanghai 200025, China*
[3] *Institute of Respiratory Diseases, Shanghai Jiao Tong University School of Medicine, Shanghai 200025, China*

Cite this article: *Nano Research*, **2025**, *18*, 94907906. https://doi.org/10.26599/NR.2025.94907906

ABSTRACT: The development of nanomedicine that can be efficiently internalized by drug-resistant cancer cells still presents a daunting challenge due to the low uptake capacity caused by various drug resistance-related factors on the cell membrane. Herein, we engineered the surfaces of glycan nanocarriers with negative, neutral, and gradient positive charges, and discovered that positively charged nanocarriers can be anchored onto the cell membrane through electrostatic attraction and thus be efficiently internalized by drug-resistant cancer cells. In contrast, drug-resistant cancer cells do not readily uptake neutral or negatively charged nanocarriers. By proposing a concentric ring fluorescence coefficient (CRFC), we were able to quantify the cell membrane anchoring capabilities of the nanocarriers and found that positively charged nanocarriers have a much stronger anchoring ability toward drug-resistant cell membranes than their neutral and negatively charged counterparts. Interestingly, with the increase of positive charge, the ability of the nanocarriers to become anchored onto cell membranes was further enhanced, thus confirming that electrostatic attraction plays a crucial role in the membrane-anchoring guided cellular uptake. The method of endowing nano-objects with this charge-attracting capability towards negatively charged cell membranes to drive membrane-anchoring mediated cellular uptake illustrates its potential as a universal strategy for engineering nanocarriers to promote the uptake of nanodrugs into drug-resistant cancer cells and thus improve the therapeutic effect.

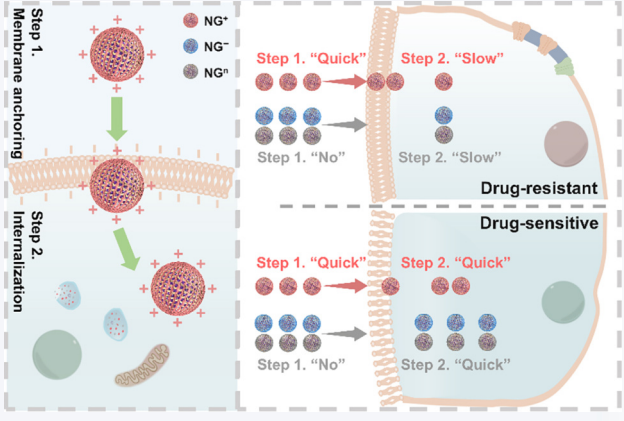

KEYWORDS: electrostatic attraction, membrane anchoring, glycan nanocarriers, drug-resistant cancer cells, concentric ring fluorescence coefficient

1 Introduction

With growing insights into cancer, the development of drug resistance, a natural outcome as tumors evolve, has emerged as a major obstacle impeding effective treatment [1–5]. Despite significant advances in understanding the mechanisms of cancer drug resistance, including tumor heterogeneity and changes in gene and protein profiles, detecting and overcoming drug resistance remains a daunting challenge [6–9]. In recent years, researchers have developed nanomedicines and some innovative drugs to combat cancer chemotherapy resistance [10–19]. However, due to the overexpression of drug resistance-related proteins and the intrinsic specificity of drug-resistant cells, both small-molecule drugs and nanomedicines cannot readily enter these cells, limiting their therapeutic impact [20, 21].

Given the generally negative charge and unique drug-pumping property of drug-resistant cell membranes [21–23], the role of surface charge engineering in the design of nanomedicines across various fields has proven to be crucial. Influenced by different

Received: June 7, 2025; **Revised:** August 6, 2025
Accepted: August 7, 2025

✉Address correspondence to Min Zhou, doctor_zhou_99@163.com; Hongjing Dou, hjdou@sjtu.edu.cn

surface charges, systematically engineered lipid nanoparticles can achieve redistribution in various organs and perform selective tissue-specific gene delivery and therapy [24, 25], and some studies have also indicated that the sub-organ biodistribution of gold nanoparticles is related to their surface charge [26]. Regarding cellular uptake, nanoparticles with different charges generally have distinct characteristics [27–36]. Among them, some cationic nanoparticles and polymers are believed to promote cellular endocytosis through their positive charge [37–43], yet the understanding of their mechanisms of action in the perimembrane region remains limited [44]. And considering some nanoparticles' morphologies and structures, some studies on nanoparticles may not necessarily be applicable to the use as nanocarriers for diagnostic or therapeutic applications. On the other hand, cationic nanoparticles often induce membrane depolarization [45], generate hydrophilic membrane pores [46, 47], and disrupt membrane structure due to strong electrostatic interactions with the cell membrane [48], which can be accompanied by significant cytotoxicity [49–53]. Moreover, most of the researches have focused on common cancers, where notable progress and success have been achieved, while research on drug-resistant cancers that emerge after cancer treatment becomes one of the most urgent challenges. How surface charge affects the interaction between nanomedicines and cells at the subcellular level, especially its potential to regulate the uptake of nanomedicines by drug-resistant cancer cells without causing cytotoxicity, remains a largely unexplored area.

Here, drawing on our recent research into the interactions and uptake mechanisms of drug-resistant cells with nano-objects [10, 13, 14], we proposed an efficient strategy for regulating the surface charge of glycan nanocarriers synthesized via a self-assembly-assisted method, while ensuring that the core component remains unchanged. By modifying the polysaccharide building blocks with varying degrees of quaternization and succinylation, we have produced a series of glycan nanocarriers that share the same interior composition and size, but exhibit a zeta potential ranging from −20 mV to approximately +60 mV. Subsequently, we delved into the mechanisms and the influence of different surface changes on the interaction between nanocarriers and drug-resistant cells. Our findings demonstrated that proposed surface engineering provides a versatile approach to effectively promote the entry of nanocarriers into drug-resistant cells through surface charge regulation, thereby paving the way for their potential adoption in both mechanistic understanding and translational applications to overcome drug resistance.

2 Results and discussion

2.1 Post-preparation surface engineering enables the construction of non-toxic glycan nanocarriers with different surface charges

Glycans are a class of biomacromolecules in living organisms with excellent biocompatibility, and the abundant functional groups on the surfaces of various glycans allow for modification with different charge groups [49, 54, 55]. To obtain charge gradient glycan nanocarriers, we modified and improved upon previous research [56, 57], utilizing the graft copolymerization-induced self-assembly (GISA) strategy to synthesize glycan nanogels with positive, negative, and neutral charges. We first employed the initiator ceric ammonium nitrate (CAN) to induce ring-opening of the polysaccharide repeating units, generating radicals that subsequently initiated the graft polymerization of the methyl acrylate monomer onto the backbones of glycan macromolecules. Then the hydrophobic-driven self-assembly force from the resulting polymethyl acrylate (PMA) chains is utilized to assemble the glycan conjugates into nanoassemblies, and N,N-methylene-bis-acrylamide (MBA) is used to crosslink and fix the assembled structure to form core-crosslinking nanogels (NGs) as nanocarriers. Moreover, surface charge regulation was achieved through the modification of functional groups on the glycan nanocarriers' surface. We designed a series of glycan nanocarriers with the same PMA core moiety but with surface changes varying in a gradient manner from negative to positive (Fig. 1(a)). The neutral nanocarriers were mainly synthesized with dextran because they lack characteristic functional groups that confer charge. On this basis, the negatively charged nanocarriers were synthesized through succinylation of chitosan oligosaccharides nanocarriers to introduce carboxyl groups onto the surface. The positively charged nanocarriers were synthesized through the quaternization modification of chitosan oligosaccharide, and chitosan in the nanocarrier's corona endows the surface with a positive charge [58, 59].

The characterization of the most representative negatively charged, neutral, and positively charged glycan nanocarriers (denoted as NG^-, NG^n, and NG^+, respectively) showed a clear gradient in zeta potential, from −20 (for NG^-), to 0 (for NG^n), and to 38 mV (NG^+), as shown in Fig. 1(e). The transmission electron microscope (TEM) images and particle size calculations (Figs. 1(b)–1(d), and 1(f)) showed that the nanocarriers are uniformly around 70 nm in diameter with a consistent spherical shape. Meanwhile, the ^{1}H nuclear magnetic resonance (NMR) spectra confirmed the presence of characteristic functional groups that determine the charge (Figs. S1–S3 in the Electronic Supplementary Material (ESM)). Subsequently, we labeled them with Cy5.5 fluorescent molecules to render them observable under fluorescence imaging, ensuring uniform fluorescence intensity for studying their cell interactions (Fig. S4 in the ESM). When exposed to environments with complex ionic concentrations, such as phosphate buffered saline (PBS) and culture media, variations in the hydrodynamic diameter and zeta potential of different charged nanocarriers can be observed (Fig. S5 in the ESM). This is attributed to the intrinsic characteristics of dynamic light scattering measurements, which results in values that are highly sensitive to the solution environment [60, 61]. However, subsequent observations revealed that changes in zeta potential do not affect the characteristic that the interaction of nanocarriers with the cell membrane is still dominated by their surface chemical structure and charged groups, which is more accurately measurable and comparable in aqueous solutions. Then, the cytotoxicity data (Fig. S6 in the ESM) indicated that the nanocarriers exhibited minimal toxicity across all charge variants, probably due to the excellent biocompatibility of the glycan corona. Subsequently, we utilized the positively charged nanocarrier to interact with drug-resistant cells, exploring the process and mechanism of their interaction in two steps: electrostatic attraction-directed membrane anchoring, and internalization with multiple mechanisms (Fig. 1(g)).

2.2 Quantify the cell membrane anchoring capabilities of glycan nanocarriers

After co-incubating the three types of nanocarriers with

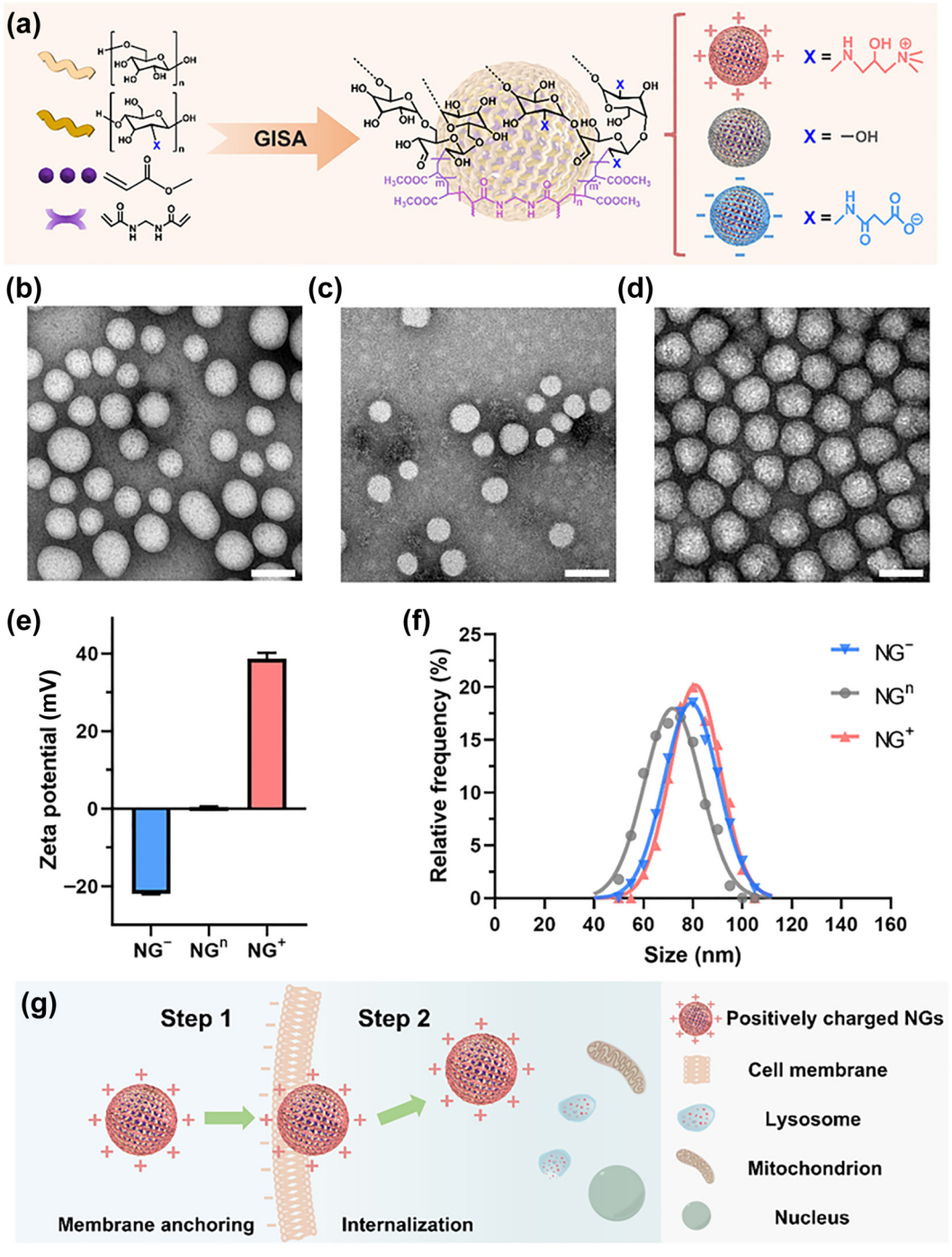

Figure 1 Schematic illustration showing the synthetic route toward glycan nanocarriers with different charge gradients along with the characterization data for these materials. (a) Schematic diagram of the synthesis and surface modification process for glycan nanocarriers with different charge gradients. TEM images of (b) NG^-, (c) NG^n, and (d) NG^+, scale bars = 100 nm. (e) Zeta potentials of NG^-, NG^n, and NG^+. Data were presented as the mean ± standard deviation (SD, n = 3). (f) The diameters of NG^-, NG^n, and NG^+ calculated from their respective TEM images. (g) Schematic illustration of positively charged nanocarriers entering drug-resistant cells in two steps.

Adriamycin-resistant breast cancer cells (MCF-7/ADR cells) for different durations, the amount of NG^- and NG^n internalized by drug-resistant cells was significantly lower than that of NG^+. Even though the fluorescence intensity increased over time, NG^+ quickly achieved a high intensity within just 5 min, which was close to the level NG^- and NG^n reached after 12 h of co-incubation (Fig. 2(a)).

As shown in Fig. 2(b), for drug-resistant cells (MCF-7/ADR cells, abbreviated as "MA" in the figures), the amount of NG^+ anchored onto the cell membrane is notably higher than that of NG^n. For drug-sensitive cells (MCF-7 cells, abbreviated as "M" on the figures), while the fluorescence intensities are similar, NG^+ is more concentrated near the cell membrane, whereas NG^n is primarily distributed within the cytoplasm. This can also be visually observed through the 3D reconstruction images in Fig. S7 in the ESM. Similar conclusions can be drawn from the line profiles of fluorescence intensity (Fig. 2(c)). In the group of positively charged nanoparticles interacting with drug-resistant cells (NG^+ → MA), the Cy5.5 fluorescence (representing NG^+) shows significant overlap

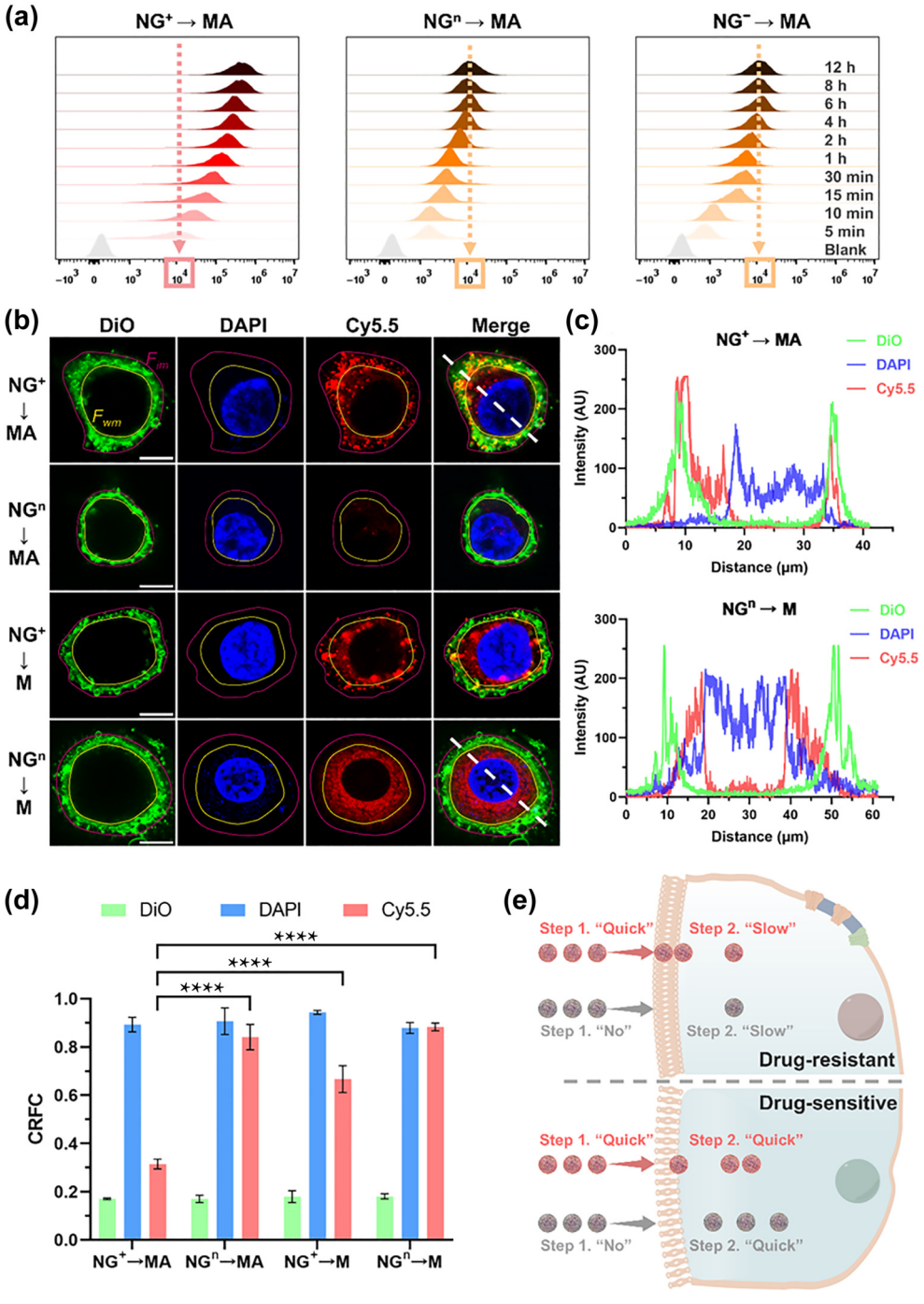

Figure 2 Internalization behavior of nanocarriers with different charge gradients in drug-resistant cells and the anchoring characteristics of NG^+ onto the cell membrane. (a) Flow cytometry data for NGs with different charge gradients (NG^-, NG^n, NG^+) co-incubated with drug-resistant cell (MA: MCF-7/ADR cell) for 5, 10, 15, and 30 min, 1, 2, 4, 6, 8, and 12 h, respectively. (b) Confocal microscope images and (d) CRFCs of NG^+ and NG^n that had been co-incubated with drug-resistant cells (MA: MCF-7/ADR cell) and drug-sensitive cells (M: MCF-7 cell) for 1 h. Scale bar = 10 μm. Statistical analysis was performed via One-Way analysis of variance (n = 3, $^*P < 0.05$, $^{**}P < 0.01$, $^{***}P < 0.001$ and $^{****}P < 0.0001$). A CRFC closer to 1 indicates that the fluorescence is primarily localized within the cell membrane, while a CRFC closer to 0 suggests that the fluorescence is mainly localized on the cell membrane. (c) Line profiles along white dashed lines in (b). DiO stains the membrane region, DAPI stains the nucleus region, and Cy5.5 represents the position of NGs. AU: arbitrary units. (e) Schematic diagram illustrating the entry of NG^+ and NG^n into drug-resistant and drug-sensitive cells, as well as the efficiency of each step.

with the DiO fluorescence (representing the cell membrane) at the membrane site. In contrast, in the NG^n → M group, the Cy5.5 fluorescence representing NG^n is predominantly observed in the cytoplasmic region between the cell membrane (DiO) and the nucleus (4',6-diamidino-2-phenylindole (DAPI)). These differences indicate distinct modes of interaction with the cells for the two types of NGs. Additionally, NG^- exhibits similar fluorescence intensity and distribution patterns to those exhibited by NG^n during cell interactions (Figs. S8–S11 in the ESM).

To better describe the localization of NGs on or within the cell

membrane, we proposed a coefficient named concentric ring fluorescence coefficient (CRFC) to quantify their cell membrane anchoring ability as shown in Eq. (1).

$$\mathrm{CRFC} = \frac{F_{\mathrm{wm}} - F_0}{F_{\mathrm{im}} - F_0} \quad (1)$$

Here F_{wm} represents the fluorescence intensity within the membrane, as indicated by the area enclosed by the yellow circle in Fig. 2(b); F_{im} represents the total fluorescence intensity including the membrane, as indicated by the area enclosed by the red circle in Fig. 2(b), and F_0 represents the background fluorescence intensity. As shown in Fig. 2(d), after NG^+ and NG^n had been co-incubated with drug-resistant MCF-7/ADR cells and drug-sensitive MCF-7 cells for 1 h, it was found that the CRFC of DiO remained consistently low across all groups (at which point F_{wm} was relatively lower compared to F_{im}), while the CRFC of DAPI remained consistently high (at which point F_{wm} and F_{im} values were quite close). This behavior matches the expected outcomes, as DiO stains the cell membrane and DAPI stains the nucleus, thus validating the usefulness of this coefficient. Now, shifting focus to the CRFC values of Cy5.5, it's evident that NG^+ is primarily located on the cell membrane in drug-resistant cells, consistent with the analogous low CRFC values of the membrane marker DiO. Conversely, in drug-sensitive cells, it is more extensively internalized into the cell, as evidenced by the higher CRFC value, which are comparable to those of the nuclear dye DAPI, suggesting localization to intracellular compartments within the plasma membrane. As for NG^n, they were mainly distributed within the interiors of both types of cells, although the amount internalized in drug-resistant cells is significantly less. This could be due to the neutral nature of uncharged nanocarriers and the unique physicochemical properties conferred by the dextran components, which primarily enable NG^n to interact with cells through endocytosis [15, 62, 63]. However, this mode of entry is considerably hindered by the special resistance traits of drug-resistant cells.

Confocal imaging and CRFC analysis revealed that NG^+ interacts mainly with the cell membrane, showing a strong affinity for anchoring onto it. They initially attach to cell membrane quickly via electrostatic interactions with the negatively charged membrane and are then gradually internalized. In contrast, NG^n lacks a strongly charged surface, and its interaction with cells is mainly dominated by normal cellular internalization, which shows "No" significant correlation with electrostatic attraction. However, in drug-resistant cells, due to the cell membrane pumping effect related to drug-resistance associated proteins as well as the denser arrangement of cell membrane phospholipids [21, 23, 64], they exhibit significant resistance behaviors against both nanoparticles and drug molecules, which leads to much slower or even greatly restricted internalization of nanocarriers. In drug-sensitive cells, while NG^+ also displays some anchoring onto the cell membrane, they are more internalized within the cell, as is the case with NG^n. This could be attributed to the stronger endocytic capacity of drug-sensitive cells, which allows for quicker internalization of various nanocarriers, as illustrated in Fig. 2(e).

2.3 Intracellular fate of glycan nanocarriers into drug-resistant cancer cells

Subsequently, we explored how NGs interact with both drug-resistant and drug-sensitive cancer cells over time, and tracked their complete uptake, circulation, and ultimate fate within the cells. The CRFC data of NGs co-incubated with drug-resistant and drug-sensitive cells at different time points (Figs. 3(a) and 3(b)) indicated that NG^+ was initially retained on the cell membrane, and then rapidly entered drug-sensitive cells, while in the case of drug-resistant cells, the entry was slower and less efficient. NG^n showed high CRFC values in both cells, indicating that it was internalized via endocytosis irrespective of the co-incubation duration. This offers a new approach to evaluate nanocarrier-cell interactions beyond just fluorescence intensity, highlighting the ease with which positively charged nanoparticles enter cells.

Furthermore, we explored the intracellular fate of NG^+ after entering drug-resistant and drug-sensitive cells. Figures 3(c) and 3(d) and Figs. S12–S14 in the ESM demonstrated that NG^+ tends to accumulate in regions associated with the cytoskeleton, specifically actin and tubulin proteins. Actin is closely aligned with the cell membrane [65–67], whereas tubulin supports the cell membrane from the inner side [68]. The relative localization of NG^+ and tubulin indicated that NG^+ appears to be resisted by actin proteins and microtubule [69], as demonstrated by the gray arrow in Figs. 3(c) and 3(d). This could be attributed to the inherent negative charge of actin and tubulin, which may cause the retention of NG^+ in the cytoskeleton-membrane areas through electrostatic attraction [70–73]. Moreover, even after 4 h of co-incubation, a considerable portion of NG^+ entered drug-resistant cells without showing notable co-localization with lysosomes (Fig. 3(e), and Fig. S15 in the ESM). This behavior suggested that NG^+ may have escaped the lysosomes or that there are additional pathways for entry into the cells beyond the typical endocytosis-endosome-lysosome route [74, 75].

2.4 Internalization mechanisms of glycan nanocarriers into drug-resistant cancer cells

Thus, we delved into the mechanisms affecting the interaction between NGs and drug-resistant cells. These factors can be grouped into three major categories: endocytic pathways, cytoskeleton, and P-glycoprotein-related decreased cell membrane fluidity (Figs. 4(a) and 4(b)). To start, by employing a series of conventional endocytosis inhibitors (Fig. S16 in the ESM) and some typical cytoskeletal protein inhibitors, we identified several inhibitors that exerted a significant restrictive effect on both NGs: chlorpromazine (CPZ), a clathrin-mediated endocytosis inhibitor [76]; dynasore (Dy), a dynamin inhibitor that affects various endocytic behaviors and cytoskeleton structures [77, 78]; and latrunculin A (LA), an F-actin polymerization inhibitor that affects the cytoskeleton [79–81]. These indicated that clathrin-mediated endocytosis is one of the mechanisms by which NGs enter drug-resistant cells, and the cytoskeleton also plays a crucial role in the interactions. By modulating cytoskeletal proteins, such as inhibiting F-actin polymerization, the cytoskeletal architecture can be significantly altered, thereby profoundly influencing the pathways and extent of NGs internalization in drug-resistant cells. Given the extensive research on the characteristic p-glycoprotein (P-gp) in drug-resistant cells, we employed two P-gp inhibitors, Tariquidar (TRQ) and Rapamycin (RAPA) [82–85]. Excitingly, they enhanced the fluorescence intensity of NGs in drug-resistant cells (Fig. 4(a)). Our previous research also mentioned similar effects [10], suggesting that this enhancement might be due to the increased cell membrane fluidity caused by P-gp inhibitors.

High P-gp activity is typically linked with decreased cell membrane fluidity [86–89]. As illustrated in Fig. S17 in the ESM, drug-resistant cancer cells overexpress P-gp, while drug-sensitive

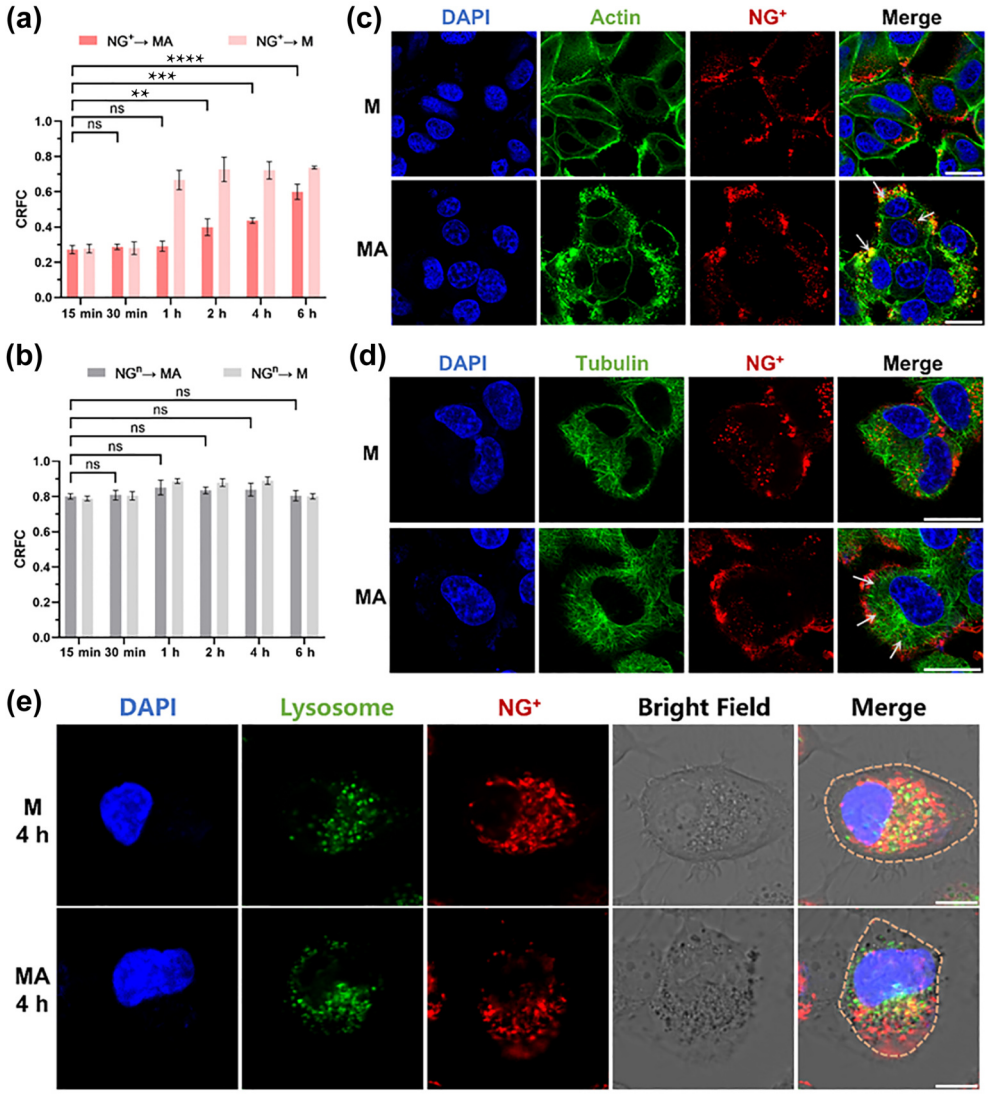

Figure 3 The intracellular fate and entry behavior of nanocarriers with different charge gradients into cancer cells. (a) CRFC of NG^+ and (b) NG^n that had been co-incubated with drug-resistant cancer cells (MA: MCF-7/ADR cells) and drug-sensitive cancer cells (M: MCF-7 cells) for 15, and 30 min, 1, 2, 4, and 6 h, respectively. (c) Confocal microscope images of NG^+ co-incubated with drug-sensitive cancer cells (M: MCF-7 cells) and drug-resistant cancer cells (MA: MCF-7/ADR cells) for 1 h, and staining with actin for co-observation. Scale bar = 20 μm. (d) Confocal microscope images of NG^+ co-incubated with drug-sensitive cancer cells (M: MCF-7 cells) and drug-resistant cancer cells (MA: MCF-7/ADR cells) for 1 or 2 h, and staining with tubulin for co-observation. Scale bar = 20 μm. (e) Confocal microscope images of NG^+ co-incubated with drug-sensitive cancer cells (M: MCF-7 cells) and drug-resistant cancer cells (MA: MCF-7/ADR cells) for 4 h, and staining with Lysosome for co-observation. Scale bar = 10 μm.

cells and normal cells express negligible P-gp. Correspondingly, we primarily utilized three methods to measure and cross-validate cell membrane fluidity. The fluorescence recovery after photobleaching (FRAP) method (Fig. S18 in the ESM) mainly measured membrane fluidity by observing the recovery behavior of fluorescence at a specific point on the membrane following photobleaching [90]. And we also assessed the membrane fluidity using the fluorescence polarization anisotropy of 1,6-diphenyl-1,3,5-hexatriene (DPH) [91–93]. Increased anisotropy indicates restricted motion of the phospholipid acyl chains within the membrane, and consequently a higher polarization value of DPH fluorescence suggests lower membrane fluidity (Fig. 4(f), and Fig. S19 in the ESM). We confirmed that the membrane fluidity of drug-resistant cancer cells is consistently lower than that of drug-sensitive cancer cells, whereas normal cells have comparable membrane fluidity to drug-sensitive cancer cells.

Additionally, we also evaluated membrane tension using the Flipper-TR membrane tension probe, which also provides insights into cell membrane fluidity. The membrane tension can be quantitatively assessed by inserting a membrane tension probe into the phospholipid bilayer of the cell membrane and measuring its fluorescence lifetime [94, 95]. The results indicated that the membrane tension of drug-resistant cells is significantly higher than that of drug-sensitive cells and normal cells (Fig. 4(c), and Fig. S20 in the ESM), suggesting a correlation between increased membrane tension and decreased membrane fluidity. In Figs. 4(d) and 4(e), positive $\Delta\tau$ values denote increased membrane tension, while negative values indicate a decrease. After NGs had been added, the membrane tension of drug-sensitive cells and normal cells increased slightly. However, drug-resistant cells, due to their already high membrane tension, showed no significant change upon the addition of NGs. Nevertheless, these observations can still provide

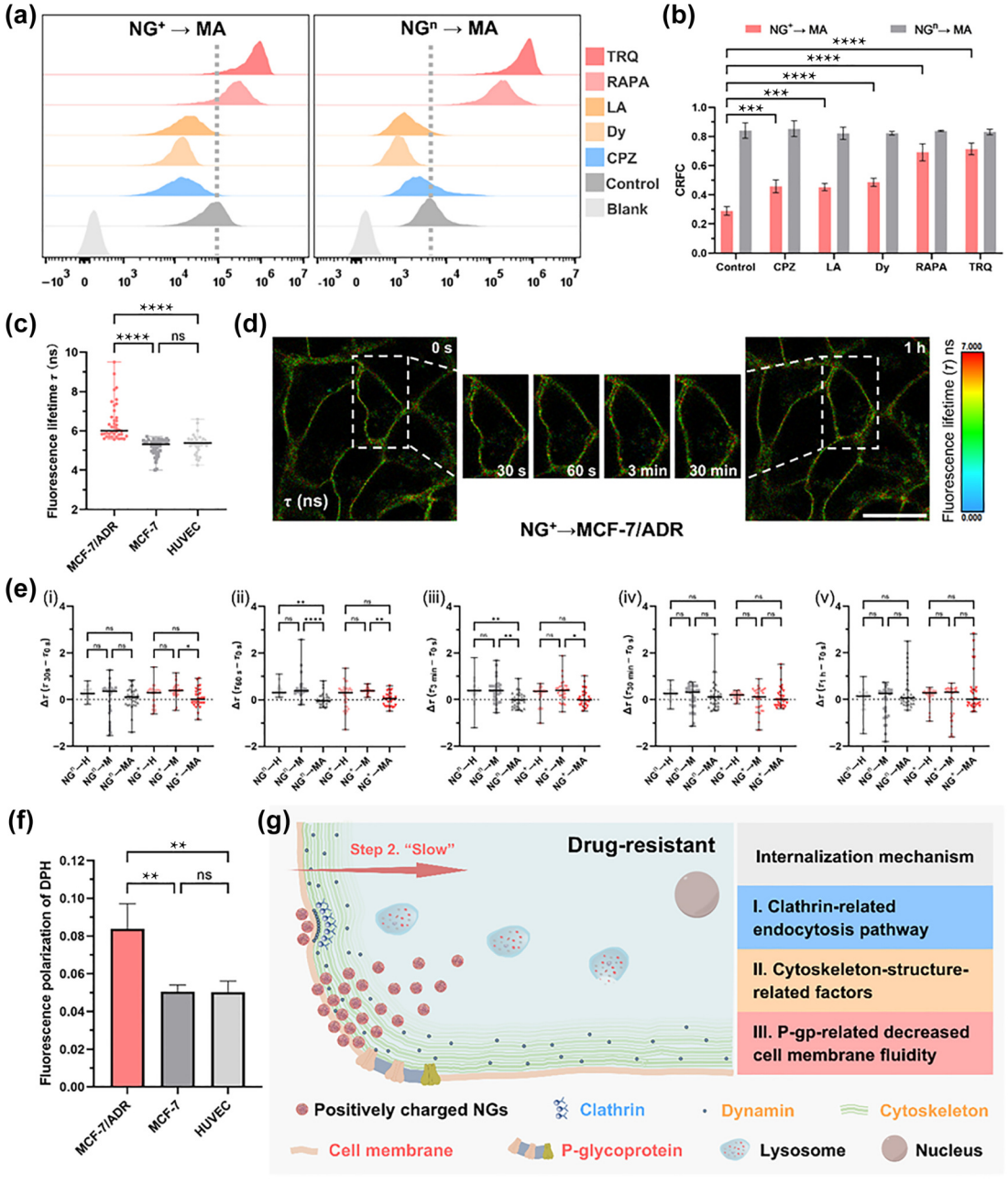

Figure 4 Mechanistic insights into the differential interactions of nanocarriers with different charges and drug-resistant cells. (a) Flow cytometry data for the cellular uptake of NG^+ and NG^n after pretreatment with various endocytosis inhibitors, cytoskeleton regulatory inhibitors, and P-gp inhibitors. All inhibitor-treated groups were compared with the untreated control group. (b) CRFC of NG^+ and NG^n co-incubated with MCF-7/ADR cells pre-treated with multiple inhibitors for 1 h. (c) Statistical graphs showing individual data points indicating fluorescence lifetime τ of 40 selected regions-of-interest (ROIs) across three biological replicates. (d) Images showing the change in fluorescence lifetime (τ) in ns of Flipper-TR probe in MCF-7/ADR cells treated with NG^+. Time-lapse images were captured at several intervals. Enlarged regions show the changes in membrane tensions of individual cells. Scale bar = 20 μm. (e) Graphs showing individual data points indicating the change in τ ($\Delta\tau$) after (i) 30 s, (ii) 60 s, (iii) 3 min, (iv) 30 min and (v) 1 h of 20 selected ROIs across three biological replicates. $\Delta\tau$ is calculated as the difference between the τ of an ROI after n seconds of NG^+ addition (τ_{ns}) minus the initial τ before NG^+ addition (τ_{0s}). MA: MCF-7/ADR cells, M: MCF-7 cells, H: HUVEC cells. Statistical analysis was performed via One-Way analysis of variance (n = 20, $^*P < 0.05$, $^{**}P < 0.01$, $^{***}P < 0.001$, and $^{****}P < 0.0001$). (f) Calculated fluorescence polarization value of DPH probe. Statistical analysis was performed via One-Way analysis of variance (n = 3, $^*P < 0.05$, $^{**}P < 0.01$, and $^{***}P < 0.001$). (g) Schematic diagram illustrating the process of NG^+ and NG^n entering drug-resistant cells and the related influencing factors.

valuable insights into the mechanistic pathways of NGs internalization, offering a potential explanation for the distinct cellular entry routes of NGs in different cell types. The changes in membrane tension upon the addition of NGs indicate that they do not significantly alter membrane tension, particularly after the initial period of pronounced fluctuations. Specifically, a large amount of NG^+ was initially anchored onto the negatively charged cell membrane (among which drug-resistant cells, due to the overexpression of glycoproteins leading to increased production of sialic acid [96, 97], have a higher negative potential, as shown in Fig. S21 in the ESM), and ultimately entered the cells through dynamic traversing process that cause significant changes in cytoskeleton and

membrane tension, but their dynamic nature and large fluctuations result in a lack of statistically significant Δt values.

To further elucidate the interaction between NGs and drug-resistant cells, we also examined the efflux behavior of NGs in drug-resistant and drug-sensitive cells, as shown in Fig. S22 in the ESM, suggesting that drug-resistant cells have a stronger efflux capacity, and highlighting the strong uptake and internalization characteristics of NG^+ in drug-resistant cells. During co-incubation, NGs were present in relative excess, as indicated by the stable fluorescence intensity (Fig. S22(a) in the ESM). After replacing the culture medium containing NGs with fresh medium and culturing the cells for 12 h, flow cytometry revealed minimal efflux in drug-sensitive cells. Conversely, the drug-resistant cells co-incubated with NG^n exhibited a gradual decrease in fluorescence, demonstrating their robust efflux capability, while those co-incubated with NG^+ maintained steady fluorescence (Fig. S22(b) in the ESM). Therefore, in our previous study, which was primarily conducted under 1 h co-incubation conditions, the low fluorescence intensity of NG^n observed within drug-resistant cells was mainly not due to efflux behavior. Although it is widely acknowledged that efflux pump proteins, such as P-glycoprotein, typically expel molecular-level substances [98–101], and affect the exocytosis of some dendritic polymers [102], we hypothesize that the drug-resistant cells characterized by their resistance-related proteins, decreased cell membrane fluidity and unique cytoskeletal structures (as evidenced by the distinct actin patterns in Fig. S14 in the ESM), may also possess an enhanced ability to expel or resist foreign nanoparticles. Surprisingly, NG^+ can overcome this efflux behavior better than NG^n (Fig. S22(b) in the ESM), and thus our focus is on the entry mechanisms of these nanocarriers into the cells.

Furthermore, we calculated the CRFC values for the interaction between NGs and drug-resistant cells following treatment with the aforementioned inhibitors (Fig. 4(b)). The impact of these inhibitors has more or less altered the distribution of NGs on the membrane or their internalization into the cells, which is also associated with changes in membrane properties that lead to variations in internalization capacity. For NG^n, inhibitor treatment did not alter its mode of internalization but only affected the quantity entering the cells. In contrast, for NG^+, the CRFC values increased to varying degrees, indicating that the three inhibitors with general inhibitory effects slightly affected the distribution of NG^+, while the two P-gp inhibitors significantly enhanced the process of NG^+ entering the cells. This suggests that P-gp inhibitors increase the membrane fluidity of drug-resistant cells, facilitating easier NGs entry, which is also the primary reason for the notable increase in fluorescence intensity (Fig. 4(a)). All these influences are summarized in Fig. 4(g).

2.5 Membrane-anchoring directed cellular uptake as a universal strategy for potentially overcoming cancer resistance

To gain insights into how nanocarriers with varying positive charge gradients interact with different cell types, and to develop a universally applicable platform for studying drug-resistant cells, we further designed two types of positively charged nanocarriers by controlling the quaternization degree and polysaccharide ratios. The main components of this series of positively charged nanocarriers are quaternized chitosan oligosaccharides (qCOS) and quaternized chitosan (qCS), with their ^{1}H NMR spectra provided in Fig. S23 in the ESM. The quaternization degrees of substitution for qCS, qCOS-1, and qCOS-2, corresponding to NG^{+55}, NG^{+38}, and NG^{+17}, are 50%, 43%, and 34%, respectively (Table S1 in the ESM). Notably, NG^{+38} is the same as the previously mentioned NG^+. The TEM images, hydrated dynamic diameters, and zeta potentials of these nanocarriers are presented in Fig. 5(a) and Figs. S24 and S25 in the ESM. Figure S26 in the ESM illustrates the zeta potential stability of the NGs with different charge gradients over seven days.

To verify the interaction patterns between NGs with different charge gradients and various cells, we co-incubated all these NGs with MCF-7/ADR (drug-resistant), MCF-7 (drug-sensitive), and HUVEC (normal) cells for 1 h, and the calculated CRFC was shown in Fig. 5(b). The results revealed a consistent trend: positively charged nanocarriers exhibit a significantly higher anchoring rate on the cell membrane compared to negatively charged and uncharged nanocarriers. This effect is more pronounced in drug-resistant cells, while drug-sensitive cells and normal cells show relatively similar behaviors. Moreover, as the charge intensity increases, the anchoring rate of positively charged nanocarriers on all types of cell membranes also increases.

To further investigate the impact of pure charge gradients on the interaction between nanocarriers and cells, we conducted the co-incubation experiments at 4 °C, thereby minimizing various normal biological activities of the cells themselves and the energy-dependent processes such as endocytosis [103], and compared them with the results obtained from experiments conducted at 37 °C. As presented in Figs. 5(c) and 5(d), at 37 °C, the fluorescence intensity and distribution of NGs in drug-resistant and drug-sensitive cells are similar to what was previously described, with the uptake of NGs in drug-resistant cells varying according to surface charge, while drug-sensitive cells, primarily relying on endocytosis for NGs entry, maintained high fluorescence levels. At 4 °C, the behavior of these nanocarriers in both cells became more similar, and the fluorescence intensity showed a gradient correlation with the nanocarriers' surface charge. And overall, the fluorescence intensity at 4 °C is correspondingly lower than that at 37 °C.

Considering the impact of low-temperature conditions on a series of cellular physiological activities, we conducted control experiments at 4 °C to elucidate changes in membrane fluidity and P-glycoprotein activity in drug-resistant cells. A series of membrane fluidity assays (Figs. S27 and S28 in the ESM) revealed a reduction in membrane fluidity in both drug-resistant and drug-sensitive cells at 4 °C, which primarily contributed to the observed decrease in cellular uptake across all groups, particularly for NG^n and NG^- in drug-sensitive cells. In contrast, NG^+ maintained strong membrane anchoring via electrostatic interactions, exhibiting minimal susceptibility to fluidity-mediated internalization. Although P-gp activity assays (Fig. S29 in the ESM) indicated partial inhibition of P-gp function under 4 °C conditions, most P-gp retained relatively high activity. However, the influence of P-gp on membrane fluidity was outweighed by the dominant effect of temperature reduction, leading to an overall decline in fluorescence intensity in drug-resistant cells.

These results suggested that at 4 °C, the internalization process mediated by membrane fluidity and related factors is significantly restricted due to the hypothermic suppression of cellular activity, causing drug-sensitive cells to exhibit behavior resembling that of drug-resistant cells. Under these conditions, the interaction between nanocarriers and cells is predominantly driven by the properties of the charged nanocarriers themselves. Meanwhile, positively charged nanocarriers can maintain a higher presence on the cell membrane

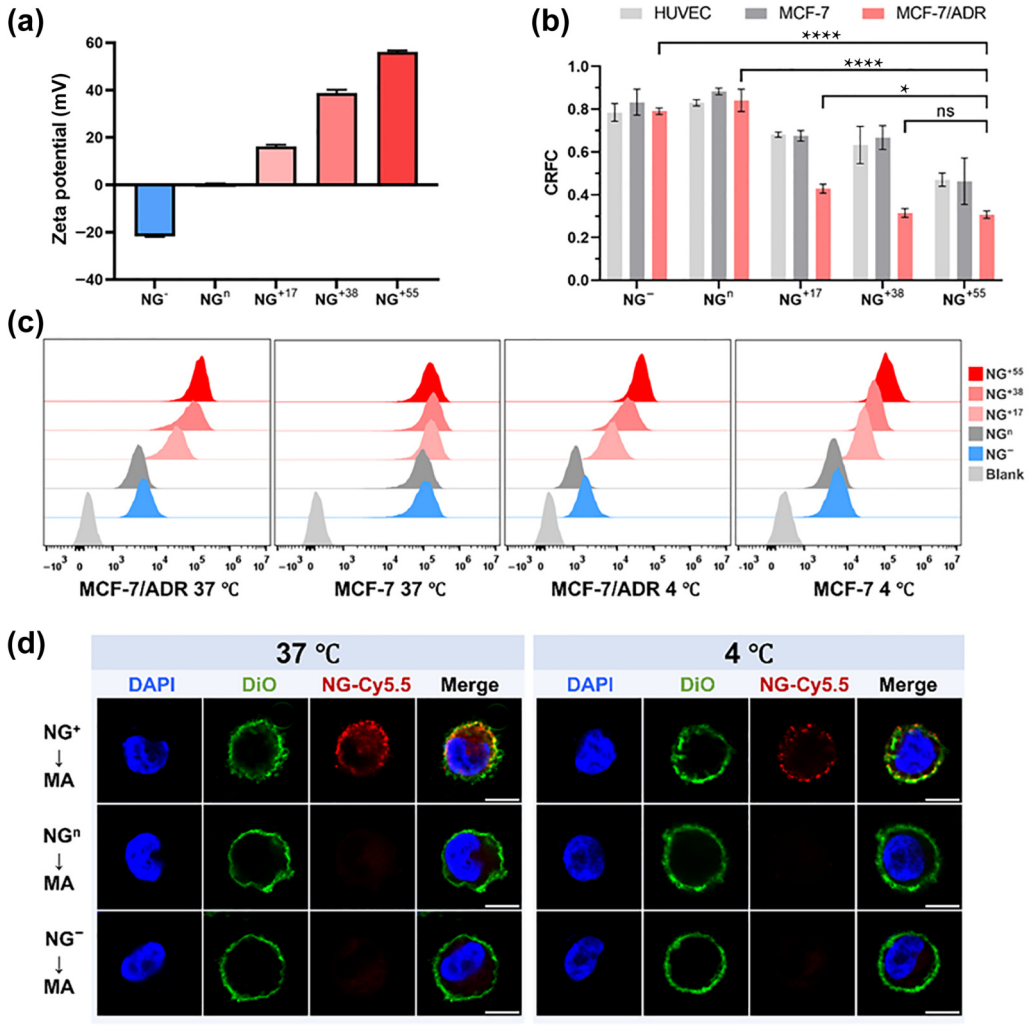

Figure 5 Exploring the regular characteristics of nanocarrier surface charge variations in their interactions with drug-resistant cells. (a) Zeta potentials of NGs with different charge gradients (NG^-, NG^n, NG^{+17}, NG^{+38}, NG^{+55}); NG^{+38} corresponds to the previously mentioned NG^+. (b) CRFCs of NGs with different charge gradients co-incubated with drug-resistant cells (MCF-7/ADR cells), drug-sensitive cells (MCF-7 cells), and normal cells (HUVEC cells) for 1 h, respectively. Statistical analysis was performed via One-Way analysis of variance ($n = 3$, $^*P < 0.05$, $^{**}P < 0.01$, $^{***}P < 0.001$ and $^{****}P < 0.0001$). (c) Flow cytometry data of NG^-, NG^n, NG^{+17}, NG^{+38}, NG^{+55} co-incubated with drug-resistant cell (MCF-7/ADR cell) or drug-sensitive cell (MCF-7) at 37 or 4 °C for 1 h. (d) Comparative confocal microscopy analysis of NG^+, NG^n, and NG^- after 1-h co-incubation with drug-resistant cancer cells (MA: MCF-7/ADR cells) at 37 or 4 °C. Scale bars = 10 μm.

through electrostatic interactions with the negatively charged cell membrane, resulting in membrane anchoring effects and higher fluorescence intensity.

Furthermore, to verify the universality of the interaction patterns between charge gradients nanocarriers and cells, we extended our investigation to various drug-resistant cancer cells (MCF-7/ADR, A549/PTX, SKOV3/PTX cells), drug-sensitive cancer cells (MCF-7, A549, SKOV3 cells), and normal cells (HUVEC cells). As shown in Figs. 6(a)–6(c), and detailed in Figs. S30–S37 in the ESM, across different cell types, nanocarriers with the same charge gradient exhibited consistent distribution behavior, demonstrating good universality. For example, in drug-sensitive cells, all charge gradient nanocarriers exhibited relatively high fluorescence intensities, while positively charged nanocarriers tend to accumulate near the cell membrane site, in contrast to the cytoplasmic enrichment observed with NG^n and NG^-. As can be quantitatively seen from Fig. 6(b), in drug-sensitive cell lines (MCF-7, A549, SKOV3, and HUVEC cells), the CRFC values of NG^+ were consistently slightly lower than those of NG^n or NG^-. However, in drug-resistant cells, negatively charged and uncharged nanocarriers exhibited significantly lower fluorescence intensities, and were nearly invisible in the confocal microscope images (Fig. 6(a)). Positively charged nanocarriers, on the other hand, maintained high fluorescence intensities, with a substantial portion anchoring on the cell membrane. This phenomenon is more prominently reflected in the low CRFC values shown in Fig. 6(b). Moreover, the CRFC values of NG^+ in drug-resistant cells were significantly different from those in the corresponding drug-sensitive group, indicating distinct distributions of NG^+ in different cell types and highlighting significant differences in cellular interactions between drug-resistant and drug-sensitive cells. This finding is consistent with our previous observations and suggests that our platform may be broadly effective across multiple cell types.

To establish the generalizability of our approach within authentic clinical models of drug resistance, here we evaluated the clinical applicability of these interaction patterns using pleural effusion specimens collected from lung cancer patients exhibiting therapeutic refractoriness. Three pleural effusions from drug-

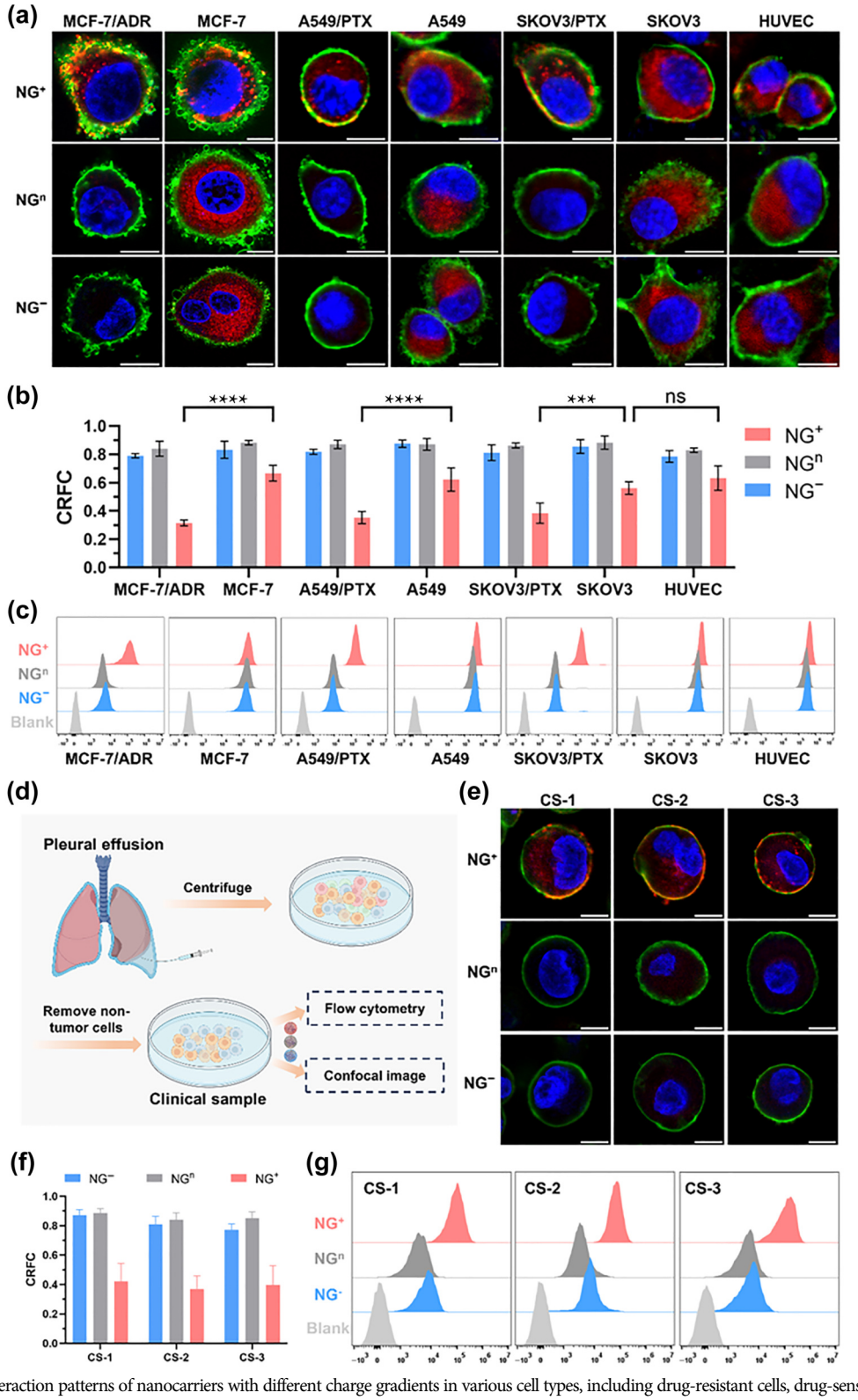

Figure 6 Universal interaction patterns of nanocarriers with different charge gradients in various cell types, including drug-resistant cells, drug-sensitive cells, and normal cells. (a) Confocal microscope images of NGs with different charge gradients co-incubated with drug-resistant cell (MCF-7/ADR cell, A549/PTX cell, and SKOV3/PTX cell), drug-sensitive cell (MCF-7 cell, A549 cell, and SKOV3 cell) and normal cell (HUVEC cell) for 1 h. Scale bar = 10 μm. (b) CRFCs of NG^+, NG^n, and NG^- co-incubated with drug-resistant cancer cells, drug-sensitive cancer cells and normal cell for 1 h, respectively. (c) Flow cytometry data of NG^+, NG^n, and NG^- co-incubated with drug-resistant cell, drug-sensitive cell and normal cell for 1 h. (d) Schematic illustrations of the treatment of pleural effusion from drug-resistant clinical samples. (e) Confocal microscope images of NGs with different charge gradients co-incubated with patient-derived cancer cells from drug-resistant clinical samples (CS-1, CS-2, and CS-3) for 1 h. Scale bar = 10 μm. (f) CRFCs of NG^+, NG^n, and NG^- co-incubated with patient-derived cancer cells (CS-1, CS-2, and CS-3) for 1 h, respectively. (g) Flow cytometry data of NG^+, NG^n, and NG^- co-incubated with patient-derived cancer cells (CS-1, CS-2, and CS-3) for 1 h. Statistical analysis was performed via One-Way analysis of variance ($n = 3$, $^*P < 0.05$, $^{**}P < 0.01$, $^{***}P < 0.001$, and $^{****}P < 0.0001$).

resistant clinical samples were processed to remove non-tumor cells and enrich patient-derived cancer cells (denoted as CS-1, CS-2, and CS-3), and then were co-incubated with NG^+, NG^n, and NG^- (Fig. 6(d)). Comprehensive characterization of patient-derived cancer cells isolated from drug-resistant clinical samples via P-glycoprotein quantification (Fig. S38(a) in the ESM) and FRAP-based membrane-fluidity analysis (Figs. S38(b)–S38(d) in the ESM) reveals that these cells exhibit markedly elevated P-glycoprotein expression (distributed non-unimodally, likely due to the heterogeneity of patient-derived cancer cells) concomitant with reduced membrane fluidity, thereby confirming their drug-resistant property. Confocal microscope images (Fig. 6(e), detailed in Figs. S39–S41 in the ESM) and the corresponding CRFC analysis (Fig. 6(f)) demonstrated that NG^+ exhibits pronounced membrane enrichment, which ensures a substantial intracellular accumulation of nanocarriers. In contrast, both NG^n and NG^- display markedly diminished fluorescence intensities—an observation corroborated by the flow-cytometric data presented in Fig. 6(g). Besides, the CRFC analysis further revealed that the diminished internalization arises from a drug-resistance-associated decline in cellular uptake competence and a consequent reduction in nanocarrier entry. Collectively, these findings substantiate the clinical applicability of the charge-gradient nanocarriers interaction paradigm with patient-derived cells, establishing a robust foundation for subsequent investigations into drug-resistance diagnostics and *in-situ* treatment of refractory cancers.

3 Conclusions

In this study, we explored the interaction patterns between nanocarriers with different surface charge gradients and heterogeneous cancer cells, especially drug-resistant cancer cells. The CRFC was proposed to quantify the cell membrane anchoring capabilities of the nanocarriers. Negatively charged and neutral nanocarriers are primarily internalized by drug-sensitive cancer cells and show significantly reduced uptake in drug-resistant cancer cells. In contrast, positively charged nanocarriers can anchor onto the cell membrane via electrostatic interactions, leading to efficient internalization by drug-resistant cancer cells. Using glycan nanocarriers with various charge gradients, we investigated the mechanisms and influencing factors of these interactions, summarizing them into three key aspects: (1) clathrin-related endocytosis pathway; (2) cytoskeleton-structure-related factors; and (3) P-glycoprotein-related decreased cell membrane fluidity. Ultimately, we extended the applicability of glycan nanocarriers with different charge gradients to various drug-sensitive and drug-resistant cancer cells, as well as to clinically relevant drug-resistant models. This suggests their potential as a generic platform for exploring and delivering *in-situ* treatment for diverse drug-resistant cancers. Moreover, by leveraging the cell membrane anchoring characteristics of highly positively charged nanocarriers, we can conduct in-depth research into cancer drug resistance behaviors and mechanisms, providing new insights for overcoming cancer.

Electronic Supplementary Material: Supplementary material (further details regarding material synthesis and operation, CRFC analysis protocol, membrane fluidity measurement, CLSM imaging, TEM imaging, flow cytometry data, P-gp measurement, etc.) is available in the online version of this article at https://doi.org/10.26599/NR.2025.94907906.

Data availability

All data needed to support the conclusions in the paper are presented in the manuscript and the Electronic Supplementary Material. Additional data related to this paper may be requested from the corresponding author upon request.

Acknowledgements

The authors wish to acknowledge financial support from the Shanghai Science and Technology Plan Project (No. 25J22800600), the National Key R&D Program of China (No. 2022YFE0100600), the National Natural Science Foundation of China (No. 21871180), the Tracking Program for Professor of Special Appointment (Eastern Scholar) at the Shanghai Institutions of Higher Learning (No. SHDP201802), the Open Project of Translational Medicine of Shanghai Jiao Tong University (Nos. TMSK-2021-108, and TMSK-2021-305), STAR Program of Shanghai Jiao Tong University (No. 20240303), and Shanghai Jiao Tong University 2030 Initiative. The authors also wish to thank the Instrumental Analysis Center (IAC) at Shanghai Jiao Tong University for providing measurements to support our experiments.

Declaration of competing interest

All the contributing authors report no conflict of interests in this work.

Author contribution statement

Q. X. G.: Theoretical work and experimental design, synthesis of the charge gradient nanocarriers, cell experiments, exploration of the cellular internalization mechanism, clinical samples. R. C.: Clinical samples. Z. T. T.: Theoretical work and experimental design, synthesis of the charge gradient nanocarriers. P. P. Z.: Synthesis of the charge gradient nanocarriers. L. S. L.: Theoretical work and experimental design, cell experiments, exploration of the cellular internalization mechanism. M. C.: Synthesis of the charge gradient nanocarriers, cell experiments. Y. R. Z.: Synthesis of the charge gradient nanocarriers. D. K. W.: Cell experiments, exploration of the cellular internalization mechanism. M. Z.: Clinical samples. H. J. D.: Conceptualization. This manuscript was written through the contributions of all authors. All authors have given approval to the final version of the manuscript.

Informed consent

Informed consents for participation were obtained from the patients.

Ethics statement

The clinical sample experiments were carried out following the guidelines of Shanghai Jiao Tong University School of Medicine for the care and use of Laboratory Animals and were approved by the Laboratory Animal Ethics Committee in Ruijin Hospital, Shanghai Jiao Tong University School of Medicine (Ethical code: AF0406/14.0/2023-03-01).

Use of AI statement

None.

References

[1] Greaves, M.; Maley, C. C. Clonal evolution in cancer. *Nature* **2012**, *481*, 306–313.

[2] Mansur, M. B.; deSouza, N. M.; Natrajan, R.; Abegglen, L. M.; Schiffman, J. D.; Greaves, M. Evolutionary determinants of curability in cancer. *Nat. Ecol. Evol.* **2023**, *7*, 1761–1770.

[3] Black, J. R. M.; McGranahan, N. Genetic and non-genetic clonal diversity in cancer evolution. *Nat. Rev. Cancer* **2021**, *21*, 379–392.

[4] Holohan, C.; Van Schaeybroeck, S.; Longley, D. B.; Johnston, P. G. Cancer drug resistance: An evolving paradigm. *Nat. Rev. Cancer* **2013**, *13*, 714–726.

[5] Gatenby, R. A.; Brown, J. S. Integrating evolutionary dynamics into cancer therapy. *Nat. Rev. Clin. Oncol.* **2020**, *17*, 675–686.

[6] Garces, A. H. I.; Porta, N.; Graham, T. A.; Banerji, U. Clinical trial designs for evaluating and exploiting cancer evolution. *Cancer Treat. Rev.* **2023**, *118*, 102583.

[7] Al-Lazikani, B.; Banerji, U.; Workman, P. Combinatorial drug therapy for cancer in the post-genomic era. *Nat. Biotechnol.* **2012**, *30*, 679–692.

[8] Vasan, N.; Baselga, J.; Hyman, D. M. A view on drug resistance in cancer. *Nature* **2019**, *575*, 299–309.

[9] Assaraf, Y. G.; Brozovic, A.; Gonçalves, A. C.; Jurkovicova, D.; Linē, A.; Machuqueiro, M.; Saponara, S.; Sarmento-Ribeiro, A. B.; Xavier, C. P. R.; Vasconcelos, M. H. The multi-factorial nature of clinical multidrug resistance in cancer. *Drug Resist. Updates* **2019**, *46*, 100645.

[10] Liu, L. S.; Zhang, Q. R.; Wang, C. L.; Guo, H. Z.; Mukwaya, V.; Chen, R.; Xu, Y. C.; Wei, X. H.; Chen, X. Y.; Zhang, S. J. et al. Single-cell diagnosis of cancer drug resistance through the differential endocytosis of nanoparticles between drug-resistant and drug-sensitive cancer cells. *ACS Nano* **2023**, *17*, 19372–19386.

[11] Wang, C. L.; Xu, X. L.; Zhang, P. P.; Xiong, S. H.; Yuan, J.; Gao, X. Z.; Guan, W. C.; Wang, F. C.; Li, X.; Dou, H. J. et al. Lipid-coated albumin-paclitaxel nanoparticles loaded with sorcin-siRNA reverse cancer chemoresistance via restoring intracellular calcium ion homeostasis. *J. Nanobiotechnol.* **2022**, *20*, 319.

[12] Wang, C. L.; Xu, X. L.; Xiong, S. H.; Zhang, P. P.; Yuan, J.; Gao, X. Z.; Guan, W. C.; Wang, F. C.; Li, X.; Leng, T. et al. Calcium-chelated nanosystem reversing cancer chemoresistance via replenishing intracellular calcium ions. *Chem. Eng. J.* **2022**, *448*, 137500.

[13] Liu, L. S.; Cheng, M.; Guo, H. Z.; Guan, Q. X.; You, J. Y.; Dou, H. J. Multidimensional quantitative measurement of cancer chemoresistance through differential ZIF-8 nanoparticle cellular retention. *ACS Appl. Mater. Interfaces* **2022**, *14*, 51798–51807.

[14] Wang, C. L.; Guan, W. C.; Peng, J. L.; Chen, Y. T.; Xu, G. X.; Dou, H. J. Gene/paclitaxel co-delivering nanocarriers prepared by framework-induced self-assembly for the inhibition of highly drug-resistant tumors. *Acta Biomater.* **2020**, *103*, 247–258.

[15] Wang, C. L.; Guan, W. C.; Chen, R.; Levi-Kalisman, Y.; Xu, Y. C.; Zhang, L. W.; Zhou, M.; Xu, G. X.; Dou, H. J. Fluorescent glycan nanoparticle-based FACS assays for the identification of genuine drug-resistant cancer cells with differentiation potential. *Nano Res.* **2020**, *13*, 3110–3122.

[16] Cao, Y.; Yang, J.; Eichin, D.; Zhao, F. Z.; Qi, D. W.; Kahari, L.; Jia, C. M.; Peurla, M.; Rosenholm, J. M.; Zhao, Z. et al. Self-synthesizing nanorods from dynamic combinatorial libraries against drug resistant cancer. *Angew. Chem., Int. Ed.* **2021**, *60*, 3062–3070.

[17] Wang, Y.; Cai, L. X.; Li, H.; Chen, H. H.; Yang, T.; Tan, Y. H.; Guo, Z. J.; Wang, X. Y. Overcoming cancer resistance to platinum drugs by inhibiting cholesterol metabolism. *Angew. Chem., Int. Ed.* **2023**, *62*, e202309043.

[18] Lin, K.; Gueble, S. E.; Sundaram, R. K.; Huseman, E. D.; Bindra, R. S.; Herzon, S. B. Mechanism-based design of agents that selectively target drug-resistant glioma. *Science* **2022**, *377*, 502–511.

[19] Lv, X. D.; Lu, X.; Cao, J.; Luo, Q.; Ding, Y.; Peng, F. L.; Pataer, A.; Lu, D.; Han, D.; Malmberg, E. et al. Modulation of the proteostasis network promotes tumor resistance to oncogenic KRAS inhibitors. *Science* **2023**, *381*, eabn4180.

[20] Kurimchak, A. M.; Herrera-Montávez, C.; Montserrat-Sangrà, S.; Araiza-Olivera, D.; Hu, J. P.; Neumann-Domer, R.; Kuruvilla, M.; Bellacosa, A.; Testa, J. R.; Jin, J. et al. The drug efflux pump MDR1 promotes intrinsic and acquired resistance to PROTACs in cancer cells. *Sci. Signal.* **2022**, *15*, eabn2707.

[21] Kopecka, J.; Trouillas, P.; Gašparović, A. Č.; Gazzano, E.; Assaraf, Y. G.; Riganti, C. Phospholipids and cholesterol: Inducers of cancer multidrug resistance and therapeutic targets. *Drug Resist. Updates* **2020**, *49*, 100670.

[22] Suetsugu, S.; Kurisu, S.; Takenawa, T. Dynamic shaping of cellular membranes by phospholipids and membrane-deforming proteins. *Physiol. Rev.* **2014**, *94*, 1219–1248.

[23] Wu, X. F.; Hu, J. J.; Yoon, J. Cell membrane as a promising therapeutic target: From materials design to biomedical applications. *Angew. Chem., Int. Ed.* **2024**, *63*, e202400249.

[24] Vaidya, A.; Moore, S.; Chatterjee, S.; Guerrero, E.; Kim, M.; Farbiak, L.; Dilliard, S. A.; Siegwart, D. J. Expanding RNAi to kidneys, lungs, and spleen via selective ORgan targeting (SORT) siRNA lipid nanoparticles. *Adv. Mater.* **2024**, *36*, 2313791.

[25] Cheng, Q.; Wei, T.; Farbiak, L.; Johnson, L. T.; Dilliard, S. A.; Siegwart, D. J. Selective organ targeting (SORT) nanoparticles for tissue-specific mRNA delivery and CRISPR-Cas gene editing. *Nat. Nanotechnol.* **2020**, *15*, 313–320.

[26] Elci, S. G.; Jiang, Y.; Yan, B.; Kim, S. T.; Saha, K.; Moyano, D. F.; Tonga, G. Y.; Jackson, L. C.; Rotello, V. M.; Vachet, R. W. Surface charge controls the suborgan biodistributions of gold nanoparticles. *ACS Nano* **2016**, *10*, 5536–5542.

[27] Mout, R.; Moyano, D. F.; Rana, S.; Rotello, V. M. Surface functionalization of nanoparticles for nanomedicine. *Chem. Soc. Rev.* **2012**, *41*, 2539–2544.

[28] Wang, J. P.; Zhang, L. Y.; Peng, F.; Shi, X. H.; Leong, D. T. Targeting endothelial cell junctions with negatively charged gold nanoparticles. *Chem. Mater.* **2018**, *30*, 3759–3767.

[29] Peter, B.; Lagzi, I.; Teraji, S.; Nakanishi, H.; Cervenak, L.; Zámbó, D.; Deák, A.; Molnár, K.; Truszka, M.; Szekacs, I. et al. Interaction of positively charged gold nanoparticles with cancer cells monitored by an *in situ* label-free optical biosensor and transmission electron microscopy. *ACS Appl. Mater. Interfaces* **2018**, *10*, 26841–26850.

[30] Zhang, H. Q.; Wei, X. R.; Liu, L.; Zhang, Q. Z.; Jiang, W. The role of positively charged sites in the interaction between model cell membranes and γ–Fe_2O_3 NPs. *Sci. Total Environ.* **2019**, *673*, 414–423.

[31] Cho, E. C.; Xie, J. W.; Wurm, P. A.; Xia, Y. N. Understanding the role of surface charges in cellular adsorption versus internalization by selectively removing gold nanoparticles on the cell surface with a I_2/KI etchant. *Nano Lett.* **2009**, *9*, 1080–1084.

[32] Feliu, N.; Parak, W. J. Developing future nanomedicines. *Science* **2024**, *384*, 385–386.

[33] Gao, J. C.; Song, Q. X.; Gu, X.; Jiang, G.; Huang, J. L.; Tang, Y. Y.; Yu, R. H.; Wang, A. T.; Huang, Y. K.; Zheng, G. et al. Intracerebral fate of organic and inorganic nanoparticles is dependent on microglial extracellular vesicle function. *Nat. Nanotechnol.* **2024**, *19*, 376–386.

[34] Zhou, Q.; Shao, S. Q.; Wang, J. Q.; Xu, C. H.; Xiang, J. J.; Piao, Y.; Zhou, Z. X.; Yu, Q. S.; Tang, J. B.; Liu, X. R. et al. Enzyme-activatable polymer-drug conjugate augments tumour penetration and treatment efficacy. *Nat. Nanotechnol.* **2019**, *14*, 799–809.

[35] Fröhlich, E. The role of surface charge in cellular uptake and cytotoxicity of medical nanoparticles. *Int. J. Nanomed.* **2012**, *7*, 5577–5591.

[36] Wang, H. X.; Zuo, Z. Q.; Du, J. Z.; Wang, Y. C.; Sun, R.; Cao, Z. T.; Ye, X. D.; Wang, J. L.; Leong, K. W.; Wang, J. Surface charge

critically affects tumor penetration and therapeutic efficacy of cancer nanomedicines. *Nano Today* **2016**, *11*, 133–144.

[37] Yen, H. J.; Young, Y. A.; Tsai, T. N.; Cheng, K. M.; Chen, X. A.; Chen, Y. C.; Chen, C. C.; Young, J. J.; Hong, P. D. Positively charged gold nanoparticles capped with folate quaternary chitosan: Synthesis, cytotoxicity, and uptake by cancer cells. *Carbohydr. Polym.* **2018**, *183*, 140–150.

[38] Roshanzadeh, A.; Park, S.; Ganjbakhsh, S. E.; Park, J.; Lee, D. H.; Lee, S.; Kim, E. S. Surface charge-dependent cytotoxicity of plastic nanoparticles in alveolar cells under cyclic stretches. *Nano Lett.* **2020**, *20*, 7168–7176.

[39] Parkinson, S. J.; Tungsirisurp, S.; Joshi, C.; Richmond, B. L.; Gifford, M. L.; Sikder, A.; Lynch, I.; O'Reilly, R. K.; Napier, R. M. Polymer nanoparticles pass the plant interface. *Nat. Commun.* **2022**, *13*, 7385.

[40] Forest, V.; Cottier, M.; Pourchez, J. Electrostatic interactions favor the binding of positive nanoparticles on cells: A reductive theory. *Nano Today* **2015**, *10*, 677–680.

[41] Hühn, D.; Kantner, K.; Geidel, C.; Brandholt, S.; De Cock, I.; Soenen, S. J. H.; Rivera_Gil, P.; Montenegro, J. M.; Braeckmans, K.; Müllen, K. et al. Polymer-coated nanoparticles interacting with proteins and cells: Focusing on the sign of the net charge. *ACS Nano* **2013**, *7*, 3253–3263.

[42] Zhang, D. S.; Teng, K. X.; Zhao, L. Y.; Niu, L. Y.; Yang, Q. Z. Ultra-small nano-assemblies as tumor-targeted and renal clearable theranostic agent for photodynamic therapy. *Adv. Mater.* **2023**, *35*, 2209789.

[43] Huo, Q.; Zhu, J. H.; Niu, Y. M.; Shi, H. H.; Gong, Y. X.; Li, Y.; Song, H. H.; Liu, Y. pH-triggered surface charge-switchable polymer micelles for the co-delivery of paclitaxel/disulfiram and overcoming multidrug resistance in cancer. *Int. J. Nanomed.* **2017**, *12*, 8631–8647.

[44] Yan, J. Q.; Zhang, N.; Zhang, Z. Z.; Zhu, W. W.; Li, B.; Li, L.; Pu, Y. J.; He, B. Redox-responsive polyethyleneimine/tetrahedron DNA/doxorubicin nanocomplexes for deep cell/tissue penetration to overcome multidrug resistance. *J. Control. Release* **2021**, *329*, 36–49.

[45] Arvizo, R. R.; Miranda, O. R.; Thompson, M. A.; Pabelick, C. M.; Bhattacharya, R.; Robertson, J. D.; Rotello, V. M.; Prakash, Y. S.; Mukherjee, P. Effect of nanoparticle surface charge at the plasma membrane and beyond. *Nano Lett.* **2010**, *10*, 2543–2548.

[46] Lin, J. Q.; Zhang, H. W.; Chen, Z.; Zheng, Y. G. Penetration of lipid membranes by gold nanoparticles: Insights into cellular uptake, cytotoxicity, and their relationship. *ACS Nano* **2010**, *4*, 5421–5429.

[47] Leroueil, P. R.; Berry, S. A.; Duthie, K.; Han, G.; Rotello, V. M.; McNerny, D. Q.; Baker, J. R. Jr. ; Orr, B. G.; Holl, M. M. B. Wide varieties of cationic nanoparticles induce defects in supported lipid bilayers. *Nano Lett.* **2008**, *8*, 420–424.

[48] Borkowska, M.; Siek, M.; Kolygina, D. V.; Sobolev, Y. I.; Lach, S.; Kumar, S.; Cho, Y. K.; Kandere-Grzybowska, K.; Grzybowski, B. A. Targeted crystallization of mixed-charge nanoparticles in lysosomes induces selective death of cancer cells. *Nat. Nanotechnol.* **2020**, *15*, 331–341.

[49] Sun, T. M.; Zhang, Y. S.; Pang, B.; Hyun, D. C.; Yang, M. X.; Xia, Y. N. Engineered nanoparticles for drug delivery in cancer therapy. *Angew. Chem., Int. Ed.* **2014**, *53*, 12320–12364.

[50] Yang, S. C.; Leong, J.; Wang, Y. M.; Sim, R.; Tan, K. H.; Chua, Y. H.; Tan, N.; Lee, A. L. Z.; Tay, J.; Yang, Y. Y. Drug-free neutrally charged polypeptide nanoparticles as anticancer agents. *J. Control. Release* **2022**, *345*, 464–474.

[51] Park, N. H.; Cheng, W.; Lai, F.; Yang, C.; de Sessions, P. F.; Periaswamy, B.; Chu, C. W.; Bianco, S.; Liu, S. Q.; Venkataraman, S. et al. Addressing drug resistance in cancer with macromolecular chemotherapeutic agents. *J. Am. Chem. Soc.* **2018**, *140*, 4244–4252.

[52] Tay, J.; Zhao, Y. L.; Hedrick, J. L.; Yang, Y. Y. Elucidating the anticancer activities of guanidinium-functionalized amphiphilic random copolymers by varying the structure and composition in the hydrophobic monomer. *Theranostics* **2021**, *11*, 8977–8992.

[53] Shao, N.; Yuan, L.; Ma, P. C.; Zhou, M.; Xiao, X. M.; Cong, Z. H.; Wu, Y. M.; Xiao, G. H.; Fei, J.; Liu, R. H. Heterochiral β-peptide polymers combating multidrug-resistant cancers effectively without inducing drug resistance. *J. Am. Chem. Soc.* **2022**, *144*, 7283–7294.

[54] Mizrahy, S.; Peer, D. Polysaccharides as building blocks for nanotherapeutics. *Chem. Soc. Rev.* **2012**, *41*, 2623–2640.

[55] Hu, Y.; Li, Y.; Xu, F. J. Versatile functionalization of polysaccharides via polymer grafts: From design to biomedical applications. *Acc. Chem. Res.* **2017**, *50*, 281–292.

[56] Wang, H.; Dai, T. T.; Li, S. L.; Zhou, S. Y.; Yuan, X. J.; You, J. Y.; Wang, C. L.; Mukwaya, V.; Zhou, G. D.; Liu, G. J. et al. Scalable and cleavable polysaccharide nanocarriers for the delivery of chemotherapy drugs. *Acta Biomater.* **2018**, *72*, 206–216.

[57] Cheng, M.; Liu, L. S.; Zhang, P. P.; Xiong, S. H.; Dou, H. J. Cell coding arrays based on fluorescent glycan nanoparticles for cell line identification and cell contamination evaluation. *ACS Appl. Mater. Interfaces* **2021**, *13*, 44054–44064.

[58] Liang, Y. Q.; Li, Z. L.; Huang, Y.; Yu, R.; Guo, B. L. Dual-dynamic-bond cross-linked antibacterial adhesive hydrogel sealants with on-demand removability for post-wound-closure and infected wound healing. *ACS Nano* **2021**, *15*, 7078–7093.

[59] Zhao, X.; Guo, B. L.; Wu, H.; Liang, Y. P.; Ma, P. X. Injectable antibacterial conductive nanocomposite cryogels with rapid shape recovery for noncompressible hemorrhage and wound healing. *Nat. Commun.* **2018**, *9*, 2784.

[60] Derjaguin, B.; Landau, L. D. Theory of the stability of strongly charged lyophobic sols and of the adhesion of strongly charged particles in solutions of electrolytes. *Acta Physicochim. U.R.S.S.* **1941**, *14*, 633–662.

[61] Butler, J. A. V. Theory of the stability of lyophobic colloids. *Nature* **1948**, *162*, 315–316.

[62] Yuan, F.; Sun, M. N.; Liu, Z. S.; Liu, H. Q.; Kong, W. J.; Wang, R.; Qian, F. Macropinocytic dextran facilitates KRAS-targeted delivery while reducing drug-induced tumor immunity depletion in pancreatic cancer. *Theranostics* **2022**, *12*, 1061–1073.

[63] Berthiaume, E. P.; Medina, C.; Swanson, J. A. Molecular size-fractionation during endocytosis in macrophages. *J. Cell Biol.* **1995**, *129*, 989–998.

[64] Zhang, X. D.; Chen, X. K.; Guo, Y. X.; Jia, H. R.; Jiang, Y. W.; Wu, F. G. Endosome/lysosome-detained supramolecular nanogels as an efflux retarder and autophagy inhibitor for repeated photodynamic therapy of multidrug-resistant cancer. *Nanoscale Horiz.* **2020**, *5*, 481–487.

[65] Zhou, A. X.; Hartwig, J. H.; Akyürek, L. M. Filamins in cell signaling, transcription and organ development. *Trends Cell Biol.* **2010**, *20*, 113–123.

[66] Stossel, T. P.; Condeelis, J.; Cooley, L.; Hartwig, J. H.; Noegel, A.; Schleicher, M.; Shapiro, S. S. Filamins as integrators of cell mechanics and signalling. *Nat. Rev. Mol. Cell Biol.* **2001**, *2*, 138–145.

[67] Pollard, T. D.; Cooper, J. A. Actin, a central player in cell shape and movement. *Science* **2009**, *326*, 1208–1212.

[68] Fletcher, D. A.; Mullins, R. D. Cell mechanics and the cytoskeleton. *Nature* **2010**, *463*, 485–492.

[69] Gudimchuk, N. B.; McIntosh, J. R. Regulation of microtubule dynamics, mechanics and function through the growing tip. *Nat. Rev. Mol. Cell Biol.* **2021**, *22*, 777–795.

[70] Kalra, A. P.; Eakins, B. B.; Patel, S. D.; Ciniero, G.; Rezania, V.; Shankar, K.; Tuszynski, J. A. All wired up: An exploration of the electrical properties of microtubules and tubulin. *ACS Nano* **2020**, *14*, 16301–16320.

[71] Raviv, U.; Needleman, D. J.; Li, Y. L.; Miller, H. P.; Wilson, L.; Safinya, C. R. Cationic liposome-microtubule complexes: Pathways to the formation of two-state lipid-protein nanotubes with open or closed ends. *Proc. Natl. Acad. Sci. USA* **2005**, *102*, 11167–11172.

[72] Baker, N. A.; Sept, D.; Joseph, S.; Holst, M. J.; McCammon, J. A. Electrostatics of nanosystems: Application to microtubules and the ribosome. *Proc. Natl. Acad. Sci. USA* **2001**, *98*, 10037–10041.
[73] Tang, J. X.; Janmey, P. A. The polyelectrolyte nature of F-actin and the mechanism of actin bundle formation. *J. Biol. Chem.* **1996**, *271*, 8556–8563.
[74] Rennick, J. J.; Johnston, A. P. R.; Parton, R. G. Key principles and methods for studying the endocytosis of biological and nanoparticle therapeutics. *Nat. Nanotechnol.* **2021**, *16*, 266–276.
[75] Montizaan, D.; Bartucci, R.; Reker-Smit, C.; de Weerd, S.; Åberg, C.; Guryev, V.; Spierings, D. C. J.; Salvati, A. Genome-wide forward genetic screening to identify receptors and proteins mediating nanoparticle uptake and intracellular processing. *Nat. Nanotechnol.* **2024**, *19*, 1022–1031.
[76] Wang, L. H.; Rothberg, K. G.; Anderson, R. G. Mis-assembly of clathrin lattices on endosomes reveals a regulatory switch for coated pit formation. *J. Cell Biol.* **1993**, *123*, 1107–1117.
[77] Macia, E.; Ehrlich, M.; Massol, R.; Boucrot, E.; Brunner, C.; Kirchhausen, T. Dynasore, a cell-permeable inhibitor of dynamin. *Dev. Cell* **2006**, *10*, 839–850.
[78] Ferguson, S. M.; De Camilli, P. Dynamin, a membrane-remodelling GTPase. *Nat. Rev. Mol. Cell Biol.* **2012**, *13*, 75–88.
[79] Ayscough, K. R.; Stryker, J.; Pokala, N.; Sanders, M.; Crews, P.; Drubin, D. G. High rates of actin filament turnover in budding yeast and roles for actin in establishment and maintenance of cell polarity revealed using the actin inhibitor latrunculin-A. *J. Cell Biol.* **1997**, *137*, 399–416.
[80] Spector, I.; Shochet, N. R.; Kashman, Y.; Groweiss, A. Latrunculins: Novel marine toxins that disrupt microfilament organization in cultured cells. *Science* **1983**, *219*, 493–495.
[81] Rotsch, C.; Radmacher, M. Drug-induced changes of cytoskeletal structure and mechanics in fibroblasts: An atomic force microscopy study. *Biophys. J.* **2000**, *78*, 520–535.
[82] Palmeira, A.; Sousa, E.; Vasconcelos, M. H.; Pinto, M. M. Three decades of P-gp inhibitors: Skimming through several generations and scaffolds. *Curr. Med. Chem.* **2012**, *19*, 1946–2025.
[83] Fox, E.; Bates, S. E. Tariquidar (XR9576): A P-glycoprotein drug efflux pump inhibitor. *Expert Rev. Anticancer Ther.* **2007**, *7*, 447–459.
[84] Kimchi-Sarfaty, C.; Oh, J. M.; Kim, I. W.; Sauna, Z. E.; Calcagno, A. M.; Ambudkar, S. V.; Gottesman, M. M. A "silent" polymorphism in the *MDR*1 gene changes substrate specificity. *Science* **2007**, *315*, 525–528.
[85] Hackstein, H.; Taner, T.; Logar, A. J.; Thomson, A. W. Rapamycin inhibits macropinocytosis and mannose receptor-mediated endocytosis by bone marrow-derived dendritic cells. *Blood* **2002**, *100*, 1084–1087.
[86] Vijayaraghavalu, S.; Peetla, C.; Lu, S.; Labhasetwar, V. Epigenetic modulation of the biophysical properties of drug-resistant cell lipids to restore drug transport and endocytic functions. *Mol. Pharm.* **2012**, *9*, 2730–2742.
[87] Hendrich, A. B.; Michalak, K. Lipids as a target for drugs modulating multidrug resistance of cancer cells. *Curr. Drug Targets* **2003**, *4*, 23–30.
[88] Peetla, C.; Vijayaraghavalu, S.; Labhasetwar, V. Biophysics of cell membrane lipids in cancer drug resistance: Implications for drug transport and drug delivery with nanoparticles. *Adv. Drug Del. Rev.* **2013**, *65*, 1686–1698.
[89] Sharom, F. J. The P-glycoprotein multidrug transporter: Interactions with membrane lipids, and their modulation of activity. *Biochem. Soc. Trans.* **1997**, *25*, 1088–1096.
[90] Rodriguez-Rivera, F. P.; Zhou, X. X.; Theriot, J. A.; Bertozzi, C. R. Visualization of mycobacterial membrane dynamics in live cells. *J. Am. Chem. Soc.* **2017**, *139*, 3488–3495.
[91] Governa, M.; Valentino, M.; Visona', I.; Rocco, M. Impairment of human polymorphonuclear leukocyte chemotaxis by 2,5-hexanedione. *Cell Biol. Toxicol.* **1986**, *2*, 33–39.
[92] Lv, Y. Q.; Xu, C. R.; Zhao, X. M.; Lin, C. S.; Yang, X.; Xin, X. F.; Zhang, L.; Qin, C.; Han, X. P.; Yang, L. et al. Nanoplatform assembled from a CD44-targeted prodrug and smart liposomes for dual targeting of tumor microenvironment and cancer cells. *ACS Nano* **2018**, *12*, 1519–1536.
[93] Cai, C. X.; Zhu, H.; Chen, J. W. Overexpression of caveolin-1 increases plasma membrane fluidity and reduces P-glycoprotein function in Hs578T/Dox. *Biochem. Bioph. Res. Commun.* **2004**, *320*, 868–874.
[94] Arafiles, J. V. V.; Franke, J.; Franz, L.; Gómez-González, J.; Kemnitz-Hassanin, K.; Hackenberger, C. P. R. Cell-surface-retained peptide additives for the cytosolic delivery of functional proteins. *J. Am. Chem. Soc.* **2023**, *145*, 24535–24548.
[95] Colom, A.; Derivery, E.; Soleimanpour, S.; Tomba, C.; Dal Molin, M.; Sakai, N.; González-Gaitán, M.; Matile, S.; Roux, A. A fluorescent membrane tension probe. *Nat. Chem.* **2018**, *10*, 1118–1125.
[96] Liu, S. W.; Wang, L.; Li, S. Y.; Meng, X. Y.; Sun, B.; Zhang, X.; Zhang, L. N.; Liu, Y.; Lin, M.; Zhang, H. et al. Multidrug resistant tumors-aimed theranostics on the basis of strong electrostatic attraction between resistant cells and nanomaterials. *Biomater. Sci.* **2019**, *7*, 4990–5001.
[97] Lehmann, F.; Tiralongo, E.; Tiralongo, J. Sialic acid-specific lectins: Occurrence, specificity and function. *Cell. Mol. Life Sci. CMLS* **2006**, *63*, 1331–1354.
[98] Fan, J. Y.; To, K. K. W.; Chen, Z. S.; Fu, L. W. ABC transporters affects tumor immune microenvironment to regulate cancer immunotherapy and multidrug resistance. *Drug Resist. Updates* **2023**, *66*, 100905.
[99] Gottesman, M. M.; Fojo, T.; Bates, S. E. Multidrug resistance in cancer: Role of ATP-dependent transporters. *Nat. Rev. Cancer* **2002**, *2*, 48–58.
[100] Szakács, G.; Paterson, J. K.; Ludwig, J. A.; Booth-Genthe, C.; Gottesman, M. M. Targeting multidrug resistance in cancer. *Nat. Rev. Drug Discov.* **2006**, *5*, 219–234.
[101] Thiebaut, F.; Tsuruo, T.; Hamada, H.; Gottesman, M. M.; Pastan, I.; Willingham, M. C. Cellular localization of the multidrug-resistance gene product P-glycoprotein in normal human tissues. *Proc. Natl. Acad. Sci. USA* **1987**, *84*, 7735–7738.
[102] Zhang, J.; Li, M. J.; Wang, M. Y.; Xu, H.; Wang, Z. X.; Li, Y.; Ding, B. Y.; Gao, J. Q. Effects of the surface charge of polyamidoamine dendrimers on cellular exocytosis and the exocytosis mechanism in multidrug-resistant breast cancer cells. *J. Nanobiotechnol.* **2021**, *19*, 135.
[103] Xiang, J. J.; Shen, Y. H.; Zhang, Y. F.; Liu, X.; Zhou, Q.; Zhou, Z. X.; Tang, J. B.; Shao, S. Q.; Shen, Y. Q. Multipotent poly(tertiary amine-oxide) micelles for efficient cancer drug delivery. *Adv. Sci.* **2022**, *9*, 2200173.